IRSTI 31.15.35 https://doi.org/10.26577/phst20261316

# Photoelectrochemical reduction and electrochemical detection of Cr(VI) using $TiO_2$ nanosheet electrodes

N.Y. Akhanova[1], A.T. Tulegenova[1*], M.B. Aitzhanov[2], M.T. Gabdullin[1], A.Zh. Iskalieva[1], Zh. Ongaibergenov[2] and A.A. Markhabayeva[1]

[1]Kazakh-British Technical University Almaty, Kazakhstan
[2]Institute of Applied Science and Information Technologies, Almaty, Kazakhstan
*e-mail: tulegenova.aida@gmail.com

(*Received April 27, 2026; received in revised form May 30, 2026; accepted June 1, 2026*)

$TiO_2$ nanosheet electrodes were successfully fabricated on fluorine-doped tin oxide (FTO) substrates via a hydrothermal method using a $TiCl_4$–HCl–$NH_4F$ system. The obtained hierarchical nanosheet morphology provides a high surface area and abundant active sites, which are favorable for electrochemical and photoelectrochemical processes. The electrochemical performance of the $TiO_2$ electrodes was investigated for both detection and reduction of hexavalent chromium (Cr (VI)), a highly toxic and hazardous pollutant in water systems. Cyclic voltammetry revealed enhanced cathodic currents and the appearance of a reduction peak in the presence of Cr (VI), confirming its electrochemical reduction. Chronoamperometric measurements demonstrated a rapid and concentration-dependent current response, with a linear detection range of 0.01–0.8 mM and a sensitivity of 0.213 $mA \cdot mM^{-1}$, and a limit of detection (LOD) of approximately 0.003 μM. Under UV illumination, a decrease in photocurrent was observed after the addition of Cr (VI), indicating the consumption of photogenerated electrons in the photoelectrochemical reduction process. This behavior confirms that Cr (VI) acts as an efficient electron acceptor, undergoing reduction to less toxic Cr (III). The combined electrochemical and photoelectrochemical results demonstrate that $TiO_2$ nanosheet electrodes can serve as multifunctional platforms for simultaneous detection and detoxification of Cr (VI). This work highlights the potential of $TiO_2$-based systems for sustainable water purification and environmental remediation, contributing to the development of clean water technologies.

**Keywords:** $TiO_2$ nanosheets, photoelectrochemical reduction, Cr (VI); electrochemical detection, water purification.

## 1. Introduction

Hexavalent chromium (Cr (VI)) is one of the most toxic and hazardous heavy metal pollutants, widely found in industrial wastewater from electroplating, leather processing, and textile industries. Due to its high solubility, mobility, and strong oxidizing nature, Cr (VI) poses severe risks to human health and the environment, including carcinogenic and mutagenic effects [1,2].

Among various approaches for chromium remediation, the reduction of Cr (VI) to trivalent chromium (Cr (III)) is considered an effective detoxification strategy, as Cr (III) is significantly less toxic and can be easily precipitated as hydroxides. Therefore, the development of efficient materials capable of both detection and reduction of Cr (VI) is of great importance [3,4].

Titanium dioxide ($TiO_2$) has been extensively studied as a photoactive material due to its excellent chemical stability, low cost, and strong photocatalytic properties. Under UV illumination, $TiO_2$ generates electron–hole pairs [5-7], enabling redox reactions at the surface. In particular, photogenerated electrons can participate in the reduction of Cr(VI), making $TiO_2$ a promising candidate for photoelectrochemical detoxification processes[6,7].

In addition to photocatalysis, $TiO_2$-based nanostructures have attracted attention for electrochemical sensing applications due to their large surface area and favorable charge transport properties. The combination of sensing and catalytic functionality in a single material offers a promising approach for

simultaneous detection and removal of toxic species [8-10].

Although various $TiO_2$-based nanostructures such as nanotubes, nanoparticles, thin films, and heterostructures have been previously investigated for Cr (VI) sensing and photoelectrochemical reduction, many reported systems require multistep fabrication procedures, noble metal modification, or complex multicomponent architectures to achieve enhanced performance. In contrast, the present work focuses on hydrothermally synthesized $TiO_2$ nanosheets with a hierarchical layered morphology providing a large exposed surface area, abundant active sites, and facilitated charge/electrolyte transport. In addition, the proposed $TiO_2$ nanosheet platform combines dual functionality, enabling both electrochemical detection and photoelectrochemical reduction of Cr (VI) within a single material system without the use of additional cocatalysts or noble metals.

In this work, $TiO_2$ nanosheet electrodes were synthesized via a hydrothermal method on FTO substrates and investigated for both electrochemical detection and photoelectrochemical reduction of Cr(VI). The electrochemical behavior, sensing performance, and reduction mechanism were systematically studied using cyclic voltammetry, chronoamperometry, and photoelectrochemical measurements.

## 2. Materials and methods

### *2.1 Synthesis of $TiO_2$*

$TiO_2$ nanosheets were grown on FTO substrates via a hydrothermal method. Prior to synthesis, the FTO substrates (2 × 3 cm) were sequentially cleaned in acetone, isopropanol, and deionized water for 10 min each using ultrasonication. The substrates were then dried and optionally treated with UV-ozone to improve surface wettability. The growth solution was prepared by mixing 15 mL of deionized water and 15 mL of concentrated HCl (37%) under stirring. Subsequently, 0.10–0.20 g of $NH_4F$ was added and fully dissolved. Finally, 0.5 mL of $TiCl_4$ was slowly introduced into the solution under continuous stirring. The resulting solution was transferred into a Teflon-lined stainless steel autoclave, filled to approximately 70–80% of its volume. The cleaned FTO substrate was placed inside the autoclave at an angle (~45°) with the conductive side facing downward. The hydrothermal reaction was carried out at 180 °C for 12 h. After cooling naturally to room temperature, the samples were removed, thoroughly rinsed with deionized water and ethanol, and dried at 60–80 °C. Finally, the samples were annealed in air at 450 °C for 2 h to improve crystallinity and adhesion.

The chemicals used in this work included potassium dichromate ($K_2Cr_2O_7$, ≥99% ACS reagent), sulfuric acid ($H_2SO_4$, ≥95% ACS reagent), acetone (≥95% Laborfarma), and 1,5-diphenylcarbazide (DPC ≥99% Sigma Aldrich). All aqueous solutions were prepared using deionized water. A 10 mM Cr(VI) stock solution was prepared by dissolving $K_2Cr_2O_7$ in 0.5 M $H_2SO_4$. For colorimetric analysis, a 0.5 wt.% DPC solution was prepared by dissolving 1,5-diphenylcarbazide in acetone. All chemicals were used as received without additional purification.

### *2.2 Electrochemical measurements*

Electrochemical measurements were performed using a three-electrode configuration with the $TiO_2$/FTO sample as the working electrode, a platinum mesh as the counter electrode, and an Ag/AgCl (3 M KCl) electrode as the reference. The 0.5 M $H_2SO_4$ solution was used as electrolyte. All experiments were performed using a potentiostat (CorrTest CS310S) at room temperature. Chronoamperometric measurements were conducted at a fixed potential (0.2 V vs Ag/AgCl). After achieving a stable baseline current, successive aliquots of Cr (VI) stock solution (10 mM) were injected into the electrolyte under continuous stirring. The additions resulted in stepwise increases in Cr (VI) concentration, with cumulative concentrations of 0.01, 0.03, 0.08, 0.18, 0.28, 0.48, 0.78, and 1.18 mM. The steady-state current values were extracted from each step and used to construct a calibration curve of current response versus Cr (VI) concentration. A linear relationship was observed in the low concentration range (0.01–0.18 mM), and the sensitivity was calculated from the slope of the linear fit. After each addition, the current response was recorded until a steady-state value was reached.

Linear sweep voltammetry (LSV) measurements were performed under chopped UV illumination to evaluate the photoelectrochemical behavior of the $TiO_2$ electrode. The light source (Xe lamp) was periodically switched on and off during the potential scan. The scan rate was set to (10 mV $s^{-1}$). The photocurrent response was recorded in the absence and presence of Cr(VI) in 0.5 M $H_2SO_4$. The geometric area of the working electrode was approximately 1 $cm^2$.

## 3. Results and discussion

### *3.1 Morphology and structure*

The surface morphology of the synthesized $TiO_2$ was examined by SEM (Figure 1). At low magnification (Figure 1a), the sample exhibits a relatively uniform coverage of the FTO substrate by micro- and nanoscale structures. The structures are randomly

oriented and densely distributed across the surface. At higher magnification (Figure 1b), the morphology reveals the presence of rod-like and plate-like structures with irregular orientations. These features appear to originate from nucleation and anisotropic growth during the hydrothermal process [11]. The high-magnification image (Figure 1c) clearly shows the formation of hierarchical $TiO_2$ nanosheets composed of stacked layers with well-defined edges. Such a layered architecture provides an increased surface area and abundant active sites, which are beneficial for electrochemical processes. The hierarchical nanosheet morphology is expected to facilitate charge transfer and electrolyte diffusion due to the presence of exposed edges and interconnected layered structures. Such architecture promotes efficient interaction between Cr(VI) species and the $TiO_2$ surface, contributing to the enhanced cathodic current response observed during electrochemical measurements. In addition, the large exposed surface area and reduced charge transport pathways can improve the separation and transfer of photogenerated charge carriers under UV illumination, thereby enhancing the photoelectrochemical reduction performance.

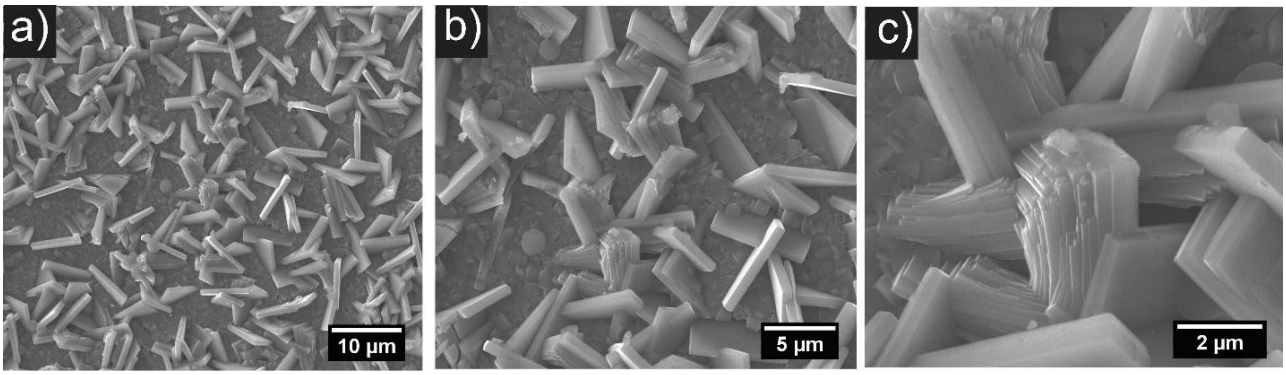


**Figure 1.** Scanning electron microscopy (SEM) images of $TiO_2$ structures grown on FTO substrate at different magnifications.

The crystalline structure of the synthesized $TiO_2$ nanosheets was investigated by X-ray diffraction (Figure 2). The diffraction pattern exhibits several well-defined peaks that can be indexed to $TiO_2$, in good agreement with the standard reference (JCPDS No. 00-001-0562). The presence of sharp and intense reflections indicates good crystallinity of the hydrothermally grown nanosheets. In addition to $TiO_2$ peaks, several diffraction signals corresponding to $SnO_2$ (JCPDS No. 01-080-6802) are observed, which originate from the FTO substrate. This confirms that the $TiO_2$ layer is relatively thin, allowing diffraction from the underlying conductive glass to be detected. No additional impurity phases were detected within the resolution of the measurement, indicating the phase purity of the synthesized $TiO_2$ nanosheets.

The structural properties of the synthesized $TiO_2$ nanosheets were further analyzed by Raman spectroscopy (Figure 3). The spectrum exhibits several characteristic peaks located at 140, 394, 514, and 636 $cm^{-1}$, which are attributed to the Eg, B1g, A1g, and Eg vibrational modes of anatase $TiO_2$, respectively. The strong and sharp Eg mode at ~140 $cm^{-1}$ indicates good crystallinity and well-defined lattice structure [12,13]. The presence of all characteristic anatase modes confirms that the hydrothermal synthesis followed by annealing resulted in phase-pure anatase $TiO_2$.

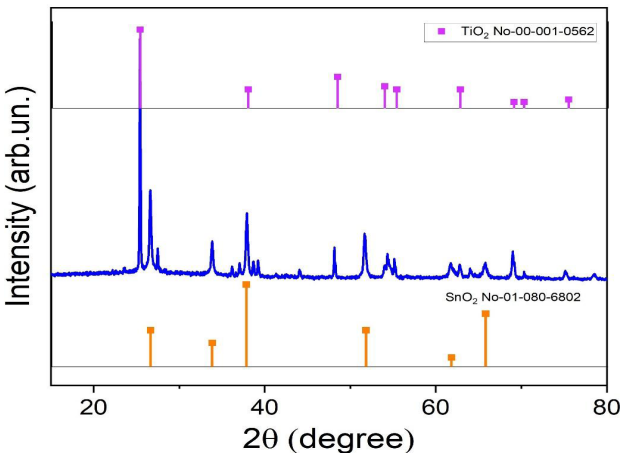


**Figure 2.** X-ray diffraction (XRD) pattern of $TiO_2$ nanosheets grown on FTO substrate.

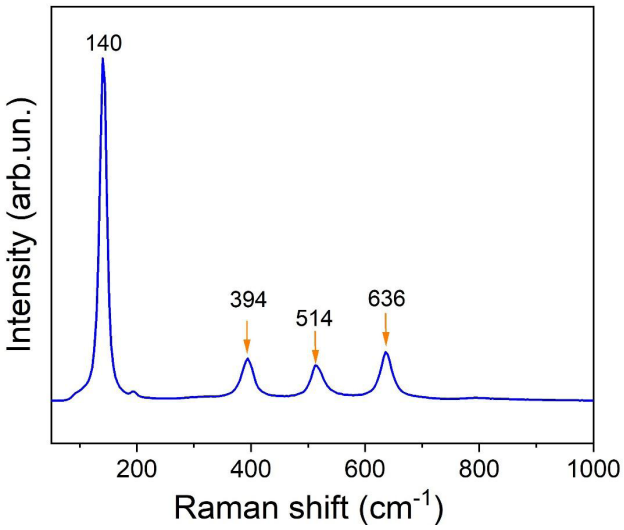


**Figure 3.** Raman spectrum of $TiO_2$ nanosheets grown on FTO substrate.

The characteristic vibrational modes are observed at 140, 394, 514, and 636 $cm^{-1}$, corresponding to the Eg, B1g, A1g, and Eg modes of anatase $TiO_2$, confirming the formation of the anatase phase.

*3.2 Electrochemical performance*

The electrochemical behavior of the $TiO_2$ electrode was investigated by cyclic voltammetry (Figure 4a). In the presence of Cr(VI), a significant increase in cathodic current is observed compared to the blank electrolyte [14]. Additionally, a reduction peak appears in the potential range of ~0.0–0.2 V vs. Ag/AgCl, indicating the electrochemical reduction of Cr (VI) to Cr (III). This confirms that the $TiO_2$ nanosheet electrode exhibits catalytic activity toward Cr (VI) reduction.

Figure 4b shows the chronoamperometric response of the $TiO_2$ electrode upon successive additions of Cr (VI). Each injection results in a sharp cathodic current drop followed by stabilization at a new steady-state level. The magnitude of the current response increases with increasing Cr (VI) concentration, indicating a concentration-dependent electrochemical response. The transient spikes are attributed to rapid mass transport and adsorption processes occurring at the electrode surface [15,16].

The steady-state current values were extracted from the chronoamperometric measurements to construct a calibration curve (Figure 4c). A linear relationship between current density and Cr (VI) concentration was observed, with a sensitivity of 0.213 $mA \cdot mM^{-1}$ and a correlation coefficient of $R^2 = 0.98$. This result demonstrates the good sensitivity of the $TiO_2$ electrode toward Cr (VI), making it suitable for electrochemical detection. The calibration plot exhibited a linear relationship between the current response and Cr (VI) concentration with a sensitivity of 0.213 mA $mM^{-1}$. The limit of detec $LOD = \frac{3\sigma}{S}$ was calculated according to the equation: , where σ is the standard deviation of the blank signal and S is the slope of the calibration curve. Based on the stable baseline region of the chronoamperometric response, the LOD was estimated to be approximately 0.01 μM.

The photoelectrochemical behavior of the $TiO_2$ electrode was further investigated under chopped UV illumination (Figure 4d). A clear photocurrent response is observed due to the generation of electron–hole pairs in $TiO_2$. After the addition of Cr (VI), a noticeable decrease in photocurrent is observed over the entire potential range. This behavior suggests that photogenerated electrons are consumed in the reduction of Cr (VI), confirming the photoelectrochemical reduction mechanism [17-19].

To further verify the reduction of Cr (VI), UV–Vis analysis using the diphenylcarbazide (DPC) method was performed before and after photoelectrochemical treatment (Figure 5). A pronounced decrease in the characteristic absorption band at ~540 nm was observed after PEC treatment, confirming the significant consumption of Cr (VI) during the reduction process.

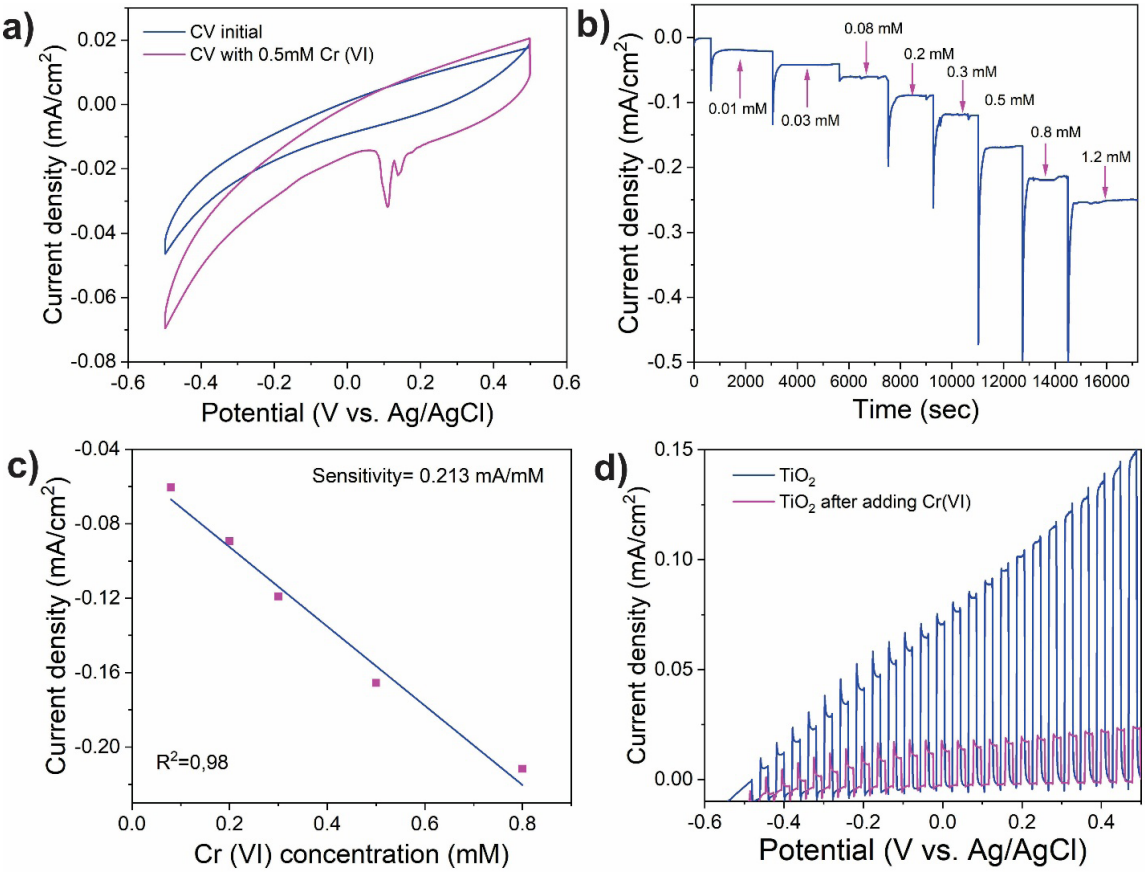


**Figure 4.** (a) Cyclic voltammetry (CV) curves of the $TiO_2$ nanosheet electrode recorded in the absence and presence of 0.5 mM Cr (VI) in 0.5 M $H_2SO_4$ electrolyte; (b) Chronoamperometric response of the $TiO_2$ nanosheet electrode upon successive additions of Cr (VI) solution at different concentrations (0.01–1.2 mM) under a constant applied potential. (c) Calibration curve of current response versus Cr (VI) concentration in the linear range of 0.01–0.18 mM; (d) Linear sweep voltammetry (LSV) curves under chopped UV illumination recorded before and after the addition of Cr (VI).

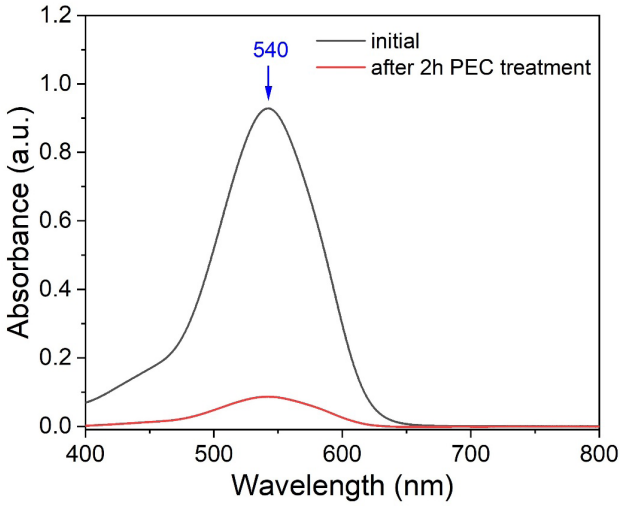


**Figure 5.** UV–Vis absorption spectra of the Cr(VI)–DPC complex before and after photoelectrochemical treatment under UV illumination.

The observed electrochemical and photoelectrochemical behavior can be explained by the role of Cr (VI) as a strong electron acceptor. Under applied potential and UV illumination, $TiO_2$ generates charge carriers (electrons and holes). The photogenerated electrons are readily transferred to Cr (VI), leading to its reduction to Cr (III) [20-26]. The schematic illustration of the proposed photoelectrochemical mechanism is presented in Figure 6. The overall process can be described as:

Cr (VI) → Cr (III)

$$TiO_2 + hv \rightarrow e^- + h^+$$

$$Cr_2O_7^{-2} + 14H^+ + 6e^- \rightarrow 2Cr^{3+} + 7H_2O$$

This electron transfer process enhances the cathodic current observed in CV and chronoampero-

metric measurements. The nanosheet architecture of $TiO_2$ further contributes to this behavior by providing improved electrode/electrolyte contact and facilitating interfacial electron transfer processes. The layered morphology also increases the accessibility of active sites for Cr(VI) adsorption and reduction. At the same time, the consumption of photogenerated electrons by Cr(VI) reduces their contribution to the external circuit, resulting in a decrease in photocurrent under UV illumination. Therefore, the presence of Cr (VI) simultaneously promotes electrochemical reduction while suppressing photocurrent, confirming its role as an efficient electron scavenger.

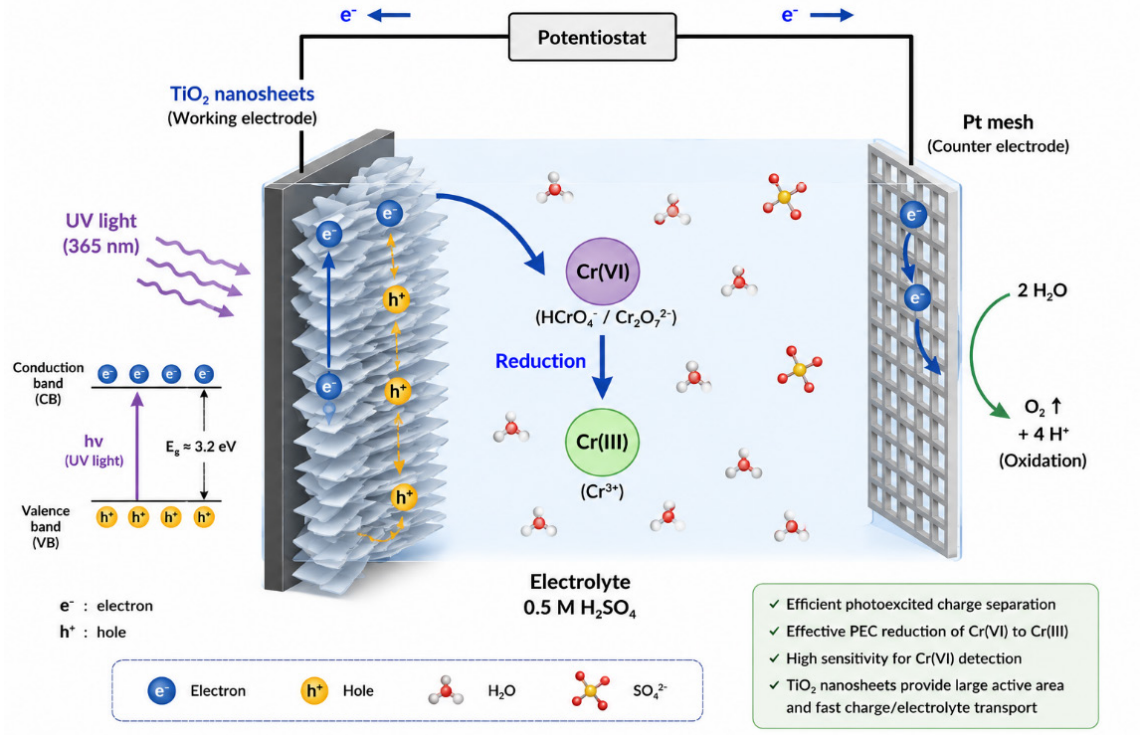


**Figure 6.** Schematic illustration of the photoelectrochemical reduction and detection mechanism of Cr (VI) on $TiO_2$ nanosheet electrodes under UV illumination.

**Table 1.** Comparison of Cr (VI) photoelectrochemical detection performance of various $TiO_2$-based and related photoelectrodes.

| Material | Detection method | Linear range | LOD | Reference |
|---|---|---|---|---|
| $TiO_2$ nanosheets | PEC reduction and electrochemical detection | 0.01–0.18 mM | 0.003 μM | This work |
| Au-decorated $TiO_2$ nanorods | PEC sensing | 0.01–50 μM | 0.006 μM | 21 |
| Screen-printed $TiO_2$ electrode | PEC sensing | 0.01–100 μM | 0.004 μM | 22 |
| $TiO_2$ nanoparticles/GQDs/PCV | PEC sensing | 0.08–100 μM | 0.04 μM | 23 |
| NiCo-LDHs/$TiO_2$ nanotube arrays | PEC sensing | 0.5–20, 20–400, 400–1800 μM | 0.12 μM | 24 |

## 4. Conclusion

Overall, the combined electrochemical and photoelectrochemical results demonstrate that $TiO_2$ nanosheet electrodes enable both the sensitive detection and efficient reduction of Cr(VI). The decrease in photocurrent under UV illumination, along with the enhanced cathodic response, confirms that Cr(VI) acts as an electron acceptor and undergoes reduction to Cr(III). The results highlight the potential of $TiO_2$

nanosheet electrodes as multifunctional platforms for environmental monitoring and detoxification. This work contributes to Sustainable Development Goal 6 (Clean Water and Sanitation) by addressing the removal and detection of toxic chromium species in aqueous systems.

**Funding**

This research was funded by the Committee of Science of the Ministry of Science and Higher Education of the Republic of Kazakhstan (Grant No. BR28712901).

**Acknowledgements**

The authors acknowledge the support of research facilities.

**Conflicts of interest**

The authors declare no conflict of interest.

**Author contributions**

Conceptualization: N.Y.A., A.T.T., A.Zh.I. and A.A.M.; Methodology: N.Y.A., A.A.M and M.B.A.; Software: M.B.A. and Zh.O.; Validation: N.Y.A., A.A.M., M.G.; Formal Analysis: A.T.T., A.Zh.I and A.A.M.; Data Curation: A.A.M., A.T.T.; Writing – Original Draft Preparation: A.A.M.; Writing – Review & Editing: N.Y.A., A.T.T and A.A.M.; Visualization: M.G.; Supervision: A.A.M.; Project Administration: A.A.M.; Funding Acquisition: N.Y.A. All authors have read and agreed to the published version of the manuscript.

**References**

1. P. Sharma, S. P. Singh, S. K. Parakh, and Y. W. Tong, "Health hazards of hexavalent chromium (Cr(VI)) and its microbial reduction," *Bioengineered*, vol. 13, no. 3, pp. 4923–4938, 2022. https://doi.org/10.1080/21655979.2022.2037273

2. S. Kerur, S. Bandekar, M. S. Hanagadakar, S. S. Nandi, G. Ratnamala, and P. G. Hegde, "Removal of hexavalent chromium: Industry treated water and wastewater—A review," *Mater. Today Proc.*, vol. 42, pp. 1112–1121, 2021. https://doi.org/10.1016/j.matpr.2020.12.492

3. S. Ambika et al., "Modified biochar as a green adsorbent for removal of hexavalent chromium from various environmental matrices: Mechanisms, methods, and prospects," *Chem. Eng. J.*, vol. 439, Art. no. 135716, 2022. https://doi.org/10.1016/j.cej.2022.135716

4. G Mussabek, S.A. Alekseev, A.I. Manilov, S. Tutashkonko, T. Nychyporuk, Y. Shabdan, G. Amirkhanova, S.V. Litvinenko, V.A. Skryshevsky, V. Lysenko, "Kinetics of Hydrogen Generation from Oxidation of Hydrogenated Silicon Nanocrystals in Aqueous Solutions," *Nanomaterials*. vol. 10, no.1413, 2020. https://doi.org/10.3390/nano10071413

5. R. Juturu, R. Selvaraj, and V. R. Murty, "Efficient removal of hexavalent chromium from wastewater using a novel magnetic biochar composite adsorbent," *J. Water Process Eng.*, vol. 66, Art. no. 105908, 2024. https://doi.org/10.1016/j.jwpe.2024.105908

6. L. Bertel, D. A. Miranda, and J. M. García-Martín, "Nanostructured titanium dioxide surfaces for electrochemical biosensing," *Sensors*, vol. 21, no. 18, Art. no. 6167, 2021. https://doi.org/10.3390/s21186167

7. G.Sh. Yar-Mukhamedova, D.M. Zellele, M. Rutkowska-Gorczyca, I. Makhambet, G. Mussabek, R. Atchibayev, A. Kemelzhanova, "Advancements in coating methods and properties of titanium based composite coatings: A review", *ES Materials and Manufacturing*, vol. 28, pp. 1669, 2025. https://dx.doi.org/10.30919/mm1569

8. J. Zhao et al., "The challenges and opportunities for $TiO_2$ nanostructures in gas sensing," *ACS Sens.*, vol. 9, no. 4, pp. 1644–1655, 2024. https://doi.org/10.1021/acssensors.4c00137

9. Y. Chen, B. Liu, Z. Chen, and X. Zuo, "Innovative electrochemical sensor using $TiO_2$ nanomaterials to detect phosphopeptides," *Anal. Chem.*, vol. 93, no. 30, pp. 10635–10643, 2021. https://doi.org/10.1021/acs.analchem.1c01973

10. G. Mussabek, N. Zhylkybayeva, S. Baktygerey, D. Yermukhamed, Ye Taurbayev, G. Sadykov, A.N. Zaderko, V.V. Lisnyak. "Preparation and characterization of hybrid nanopowder based on nanosilicon decorated with carbon nanostructures", *Applied Nanoscience*, vol.13, no.10, pp. 6709-6718. 2023. https://doi.org/10.1007/s13204-022-02681-6

11. J. M. Rzaij and A. M. Abass, "Review on $TiO_2$ thin film as a metal oxide gas sensor," *J. Chem. Rev.*, vol. 2, no. 2, pp. 114–121, 2020. https://doi.org/10.33945/SAMI/JCR.2020.2.4

12. A. Markhabayeva et al., "ZnO nanorods with GaSe nanoflakes form a heterojunction for solar water oxidation," *Appl. Surf. Sci.*, vol. 701, Art. no. 163275, 2025. https://doi.org/10.1016/j.apsusc.2025.163275

13. M. A. Ullah et al., "Facet-engineered {001} anatase $TiO_2$ nanoparticles for enhanced photocatalytic degradation of Congo Red," *J. Mol. Struct.*, 2025, Art. no. 144401. https://doi.org/10.1016/j.molstruc.2025.144401

14. B. Kuzmanović et al., "Understanding the role of interfacial PANI–$TiO_2$ interactions: A combined theoretical, spectroscopic, and electrochemical study," *J. Inorg. Organomet. Polym. Mater.*, 2026. https://doi.org/10.1007/s10904-026-04192-1

15. A. Markhabayeva, R. Dupre, R. Nemkayeva, and N. Nuraje, "Synthesis of hierarchical $WO_3$ microspheres for photoelectrochemical water splitting application," *Phys. Sci. Technol.*, vol. 10, no. 3–4, pp. 33–39, 2023. https://doi.org/10.26577/phst.2023.v10.i2.04

16. F. Bakhshandeh, S. Saha, S. Sakib, I. Zhitomirsky, and L. Soleymani, "$TiO_2$ nanoparticles co-sensitized with graphene quantum dots and pyrocatechol violet for photoelectrochemical detection of Cr(VI)," *J. Electrochem. Soc.*, vol. 169, no. 5, Art. no. 057520, 2022. https://doi.org/10.1149/1945-7111/ac6e90?urlappend=%3Futm_source%3Dresearchgate.net%26utm_medium%3Darticle

17. F. Eshaghzadeh, M. M. Momeni, and H. Farrokhpour, "Preparation of iron and chromium co-doped $TiO_2$ nanotubes and study of their photoelectrochemical properties," *J. Electron. Mater.*, vol. 52, no. 10, pp. 6977–6991, 2023.https://doi.org/10.1007/s11664-023-10596-3

18. C. Wang et al., "C-doped BiOCl/$Bi_2S_3$ heterojunction for highly efficient photoelectrochemical detection and photocatalytic reduction of Cr(VI)," *J. Mater. Sci. Technol.*, vol. 164, pp. 188–197, 2023. https://doi.org/10.1016/j.jmst.2023.03.066

19. C. V. Reddy et al., "Novel edge-capped $ZrO_2$ nanoparticles onto $V_2O_5$ nanowires for efficient photosensitized reduction of chromium (Cr(VI)), photoelectrochemical solar water splitting, and electrochemical energy storage applications," *Chem. Eng. J.*, vol. 430, Art. no. 132988, 2022. https://doi.org/10.1016/j.cej.2021.132988

20. B. Yuan et al., "Enhanced Cr(VI) stabilization by terrestrial-derived soil protein: Photoelectrochemical properties and reduction mechanisms," *J. Hazard. Mater.*, vol. 465, Art. no. 133153, 2024. https://doi.org/10.1016/j.jhazmat.2023.133153

21. R. Koutavarapu et al., "Novel Z-scheme binary zinc tungsten oxide/nickel ferrite nanohybrids for photocatalytic reduction of chromium (Cr(VI)), photoelectrochemical water splitting and degradation of toxic organic pollutants," *J. Hazard. Mater.*, vol. 423, Art. no. 127044, 2022. https://doi.org/10.1016/j.jhazmat.2021.127044

22. J. Qiao et al., "A photoelectrochemical sensor based on $TiO_2$ nanotube arrays decorated with nickel-cobalt layered double hydroxides for the effective and sensitive detection of chromium (VI)," *ACS Appl. Nano Mater.*, vol. 5, no. 4, pp. 5535–5543, 2022. https://doi.org/10.1021/acsanm.2c00521

23. H. Bahramian et al., "Enhanced Cr(VI) photoreduction in water using $TiO_2$/$CuWO_4$ photocatalytic coating," *Mater. Chem. Phys.*, vol. 354, Art. no. 132194, 2026. http://doi.org/10.1016/j.matchemphys.2026.132194

24. R. S. Moakhar, G. K. L. Goh, A. Dolati, and M. Ghorbani, "Sunlight-driven photoelectrochemical sensor for direct determination of hexavalent chromium based on Au-decorated rutile $TiO_2$ nanorods," *Appl. Catal. B Environ.*, vol. 201, pp. 411–418, 2017. https://doi.org/10.1016/j.apcatb.2016.08.026

25. R. S. Moakhar, G. K. L. Goh, A. Dolati, and M. Ghorbani, "A novel screen-printed $TiO_2$ photoelectrochemical sensor for direct determination and reduction of hexavalent chromium," *Electrochem. Commun.*, vol. 61, pp. 110–113, 2015. https://doi.org/10.1016/j.elecom.2015.10.011

26. J. Qiao, Y. Wang, Q. Liang, S. Dong, Z. Zeng, and S. Shao, "A photoelectrochemical sensor based on $TiO_2$ nanotube arrays decorated with nickel-cobalt layered double hydroxides for the effective and sensitive detection of chromium(VI)," *ACS Appl. Nano Mater.*, vol. 5, no. 4, pp. 5400–5409, 2022. https://doi.org/10.1021/acsanm.2c00521

***Information about the authors:***

*Nazym Yerlanovna Akhanova (corresponding author) – PhD, Researcher, Kazakh-British Technical University (Almaty, Kazakhstan, e-mail: n.akhanova@kbtu.kz).*

*Aida Tulegenkyzy Tulegenova – PhD, Associate Professor, Researcher, Kazakh-British Technical University (Almaty, Kazakhstan, e-mail: tulegenova.aida@gmail.com).*

*Madi Bauirzhanovich Aitzhanov – Master's degree, Researcher, Institute of Applied Science and Information Technologies (Almaty, Kazakhstan, e-mail: madi.aitzhanov@outlook.com).*

*Maratbek Gabdullin – Candidate of Sciences, Professor, Rector of the Kazakh-British Technical University (Almaty, Kazakhstan, e-mail: m.gabdullin@kbtu.kz).*

*Asylzat Zh. Iskalieva – PhD, Assistant Professor, Researcher, Kazakh-British Technical University (Almaty, Kazakhstan, e-mail: a.iskalieva@kbtu.kz).*

*Zhanserik Ongaibergenov – Researcher, Institute of Applied Science and Information Technologies, Kazakhstan (Almaty, Kazakhstan, e-mail: onajbergenovz@gmail.com).*

*Aiymkul Alikhanovna Markhabayeva – PhD, Researcher, Kazakh-British Technical University (Almaty, Kazakhstan, e-mail: aiko.marx87@gmail.com).*